



Characterization of prepared eco-friendly biochar from almond (*Terminalia catappa* L) leaf for sequestration of bromophenol blue (BPB) from aqueous solution

Jamiu Mosebolatan Jabar¹ · Ignatius Adekunle Owokotomo¹ · Yusuf Timilehin Ayinde¹ · Ayodele Modupe Alafabusuyi¹ · Gbolahan Olusayo Olagunju¹ · Victor Oluwafemi Mobolaji¹

Received: 7 September 2020 / Revised: 16 November 2020 / Accepted: 8 December 2020 / Published online: 4 January 2021
© Korean Carbon Society 2021

Abstract

Novel eco-friendly adsorbents were prepared through pyrolysis and acid activation of raw almond leaf (RAL) to form almond leaf biochar (ALB) and chemically activated almond leaf biochar (CAL), respectively. The prepared adsorbents were characterized using TGA, FTIR, SEM–EDX, BET and XRD techniques and their physicochemical properties investigated. RAL, ALB and CAL were utilized for adsorption of BPB dye from aqueous solution using batch technique under optimum conditions. The optimum dye adsorbed by RAL, ALB and CAL were 92.83, 93.21 and 94.89%, respectively at pH 3, dye initial conc. (100 mg/L), adsorbent dose (0.04 g/25 mL), 60 min contact time and 301 K adsorption temperature. Although, Langmuir maximum monolayer adsorption capacities were found to be 365.36, 535.62 and 730.46 mg/g for RAL, ALB and CAL, respectively, but isotherm conformed to Freundlich model. Kinetic study confirmed suitability of pseudo-second-order model with rate constant 9.33×10^{-4} , 9.91×10^{-4} and 12.60×10^{-4} g mg⁻¹ min⁻¹ for RAL, ALB and CAL, respectively. Negative values of thermodynamic parameters (ΔG and ΔH) established sequestration process to be spontaneous and exothermic. RAL, ALB and CAL were discovered to be highly efficient adsorbents that could be used in place of expensive commercial adsorbents.

Keywords Adsorption · Almond leaf · Batch technique · Biochar · Exothermic · Spontaneous

1 Introduction

Massive industrialization witnessed after Second World War resulted into environmental pollution, as industrial wastes and effluents were discharged directly into environment without pretreatment [1, 2]. Textile industry, which was in front line of industrialization that employed thousands of labors made use of different colors frequently (either from dyes or pigments) for different purposes, ranging from beautification, comfort, communication to worshipping to mention

but a few [3]. These coloring materials are equally used by leather, electronics, plastic, photography, cosmetic and pulp/paper industry to enhance acceptability of their products [4, 5]. BPB is one of the triphenyl methane dyes used by textile industry [6]. Contrarily to others that are generally classified as basic dyes, BPB possesses properties of acid dye due to the presence of sulfonic functional group in its chemical structure [7]. More than twenty percent (20%) of these coloring materials end up into water body as waste during the manufacturing processes and services of the finished products, there by polluting and endangering aqua-eco-system [8–10]. BPB for instance, is carcinogenic in nature and when it is found as pollutant in water it irritates skin, eye and gastrointestinal area of aquatic animals [11]. It inhibits penetration of oxygen and sunlight in water body, thereby disturbing photosynthesis of phytoplankton that serves as prey for most aquatic animals [12]. It can exist in water as pollutant for a very long time, because of its stability to sunlight, oxidation and non-biodegradable nature. Over long period of time, it may degrade into compounds that have toxic, mutagenic and

Supplementary Information The online version contains supplementary material available at <https://doi.org/10.1007/s42823-020-00214-1>.

✉ Jamiu Mosebolatan Jabar
jmjabar@futa.edu.ng

¹ Textile and Polymer Research Laboratory, Chemistry Department, The Federal University of Technology, P.M.B. 704, Akure, Nigeria

heterogenic effects on aquatic life and human beings that use the affected water body for industrial and domestic purposes [13]. Therefore, it is highly essential to sequester dye from industrial effluent before being discharged into water body to evade deadly effect that may occur in water [14]. Deferent methods have been used by many researchers to remove coloring matters and emerging contaminants from wastewater [15]. Among the methods used are biological (aerobic, anaerobic, etc.) [12], coagulation/flocculation [16], ion exchange, chemical oxidation [17], reverse osmosis [18], electrophotocatalysis, photolysis, photocatalysis degradation [19], ozonation, [20] and adsorption [8, 21]. Many of the synthetic coloring materials are not removable by biological methods, because they are not biodegradable [12]. Instead of chemical methods to remove these pollutants, they delay or increase their harmful effects in wastewater by forming another kind of pollutants in aqueous medium [22]. Therefore, it is only physical methods that can remove these pollutants from water body completely without any challenge [23]. Among the physical methods of wastewater treatment, adsorption process was considered to be the most frequent, dependable and functional technique due to its non-toxicity, easy handling, design simplicity and high efficiency to mention but a few [24, 25]. Incidentally, commercial activated carbons were widely utilized in treatment of wastewater containing coloring material [26]. On the other hand, its high price has forced researchers to be looking for cheap, sustainable and eco-friendly adsorbents from plant and animal materials for sequestration of different kind of dyes, heavy metals and emerging contaminants from wastewater [27]. Some of the plant-derived adsorbents used as replacement for eliminating pollutants from wastewater are empty fruit bunch fibre [8], elephant grass [28], moringa seed coat [29], algae [28] and cashew shell [30], just to mention a few.

Almond (*Terminalia catappa*) leaf (AL)-derived adsorbents have not been reported in wastewater treatment to the best of our knowledge. A mature Almond (*T. catappa* L) tree is about 35 m tall and 2 m wide. It has green broad leaves and flowers between 2 and 3 years of plantation [31]. Almond tree is widely planted in South-western part of Nigeria as umbrella (shade) as well as ornamental tree. Almond tree reduces transpiration rate especially during dry season by shedding off a lot of leaves daily and in turn causing environmental challenge [32]. Value can be added to this challenge, by converting fell down AL to adsorbents for treatment of wastewater. This is a means of converting waste to wealth and hereby creating indirect employment for teaming unemployed youths. The consideration of adsorbents from AL was attributed to its unique properties, such as abundance, renewable and efficient waste removal from wastewater. The activation of carbon from AL can be done through physical or/and chemical method [33]. The aim of this research work was to prepare, characterize and apply

novel eco-friendly adsorbents derived from AL as forthcoming substitutes to expensive commercially available adsorbents for sequestering BPB from its solution.

2 Experimental

2.1 Materials

Almond leaf (AL) was obtained from fell down leaves of Almond (*T. catappa* L) trees use as umbrella trees at School of Sciences, Federal University of Technology, Akure (FUTA) car parking lot and authenticated at Department of Forestry and Wood Technology, FUTA. BPB dye and all other reagents used were Analytical grade obtained from Sigma-Aldrich Chemie, Steiaheim, Germany.

2.2 Preparation of adsorbents

Adsorbents were prepared according to Jabar and Odusote [8] with little modification. AL (100 g) was cleaned thoroughly with water to get rid of dust and other related dirt. It was dried in an oven at 110 °C for 1½ h. AL (10 g) was weighed from the cleaned sample, named as raw almond leaf (RAL) and kept for further analyses. The remaining part of AL (about 90 g) was carbonized at 650 °C under inert atmosphere for 2½ h at flow rate of 150 cm³ min⁻¹ to form biochar. Biochar was then divided into two equal parts: a part was retained and named almond leaf biochar (ALB). The remaining one part of pyrolyzed carbon was soaked in conc. HNO₃ for 6 h at liquor ratio 1:10 to activate surface of biochar by enhancing the available pores, through digestion and leaching out of inorganic and related matters that might be blocking the available pores on biochar. Activated AL carbon was refluxed for 2½ h in liquor ratio 1:25 using water as solvent. Refluxed activated carbon was cooled to room temperature, decanted and soaked in 0.01 M KOH for 18 h at liquor ratio 1:10 to neutralize the acidic remnant in biochar. Activated AL biochar was decanted and washed thoroughly with water to neutral pH value; oven dried at 110 °C for 3 h and named chemical activated almond leaf biochar (CAL). RAL, ALB and CAL were then ground, sieved to mesh size between 60 and 80 µm and kept for use as adsorbents for removal of BPB dye from solution.

2.3 Characterization of adsorbents

2.3.1 pH value and iodine number (IN) determination

RAL, ALB and CAL pH values were determined according to ASTM D 3838-08, while their iodine numbers (IN) were determined according to Jabar [34]. IN of each of the samples was calculated using the following equation:

$$\text{Iodine number (IN)} = \frac{12.69(B - A)N}{W}, \quad (1)$$

where B is blank titre value in $\text{Na}_2\text{S}_2\text{O}_3$, A is sample titre value in $\text{Na}_2\text{S}_2\text{O}_3$, N is $\text{Na}_2\text{S}_2\text{O}_3$ normality and W is weight of the sample.

2.3.2 Thermal analysis

Thermogravimetric analyzer (Perkin Elmer TGA 6) was used to determine the moisture content (MC), fixed carbon content (FC), ash content (AC), volatile matter (VM) and thermal stability (TS) of RAL, ALB and CAL. Approximately 6 mg each of raw and biochar samples was placed in platinum crucible of TGA analyzer operated between temperature range 30–950 °C at a heating rate 10 °C/min under inert atmosphere. Foremost, MC of each sample was determined by raising TGA operating temperature from 30 to 115 °C and held until constant weight of the samples obtained. VM content of each sample was determined from change in weight observed when operating temperature increased to 920 °C and held for 10 min in TGA analyzer. FC was determined from change in weight observed when temperature of each of the samples was cooled from 920 to 800 °C at cooling of 20 °C/min and switched inert environment to oxygen at flow rate of 50 mL/min and held for 20 min. The leftover ash was obtained as AC that represented inorganic matter in each sample according to Idowu and Fletcher [35]. These information were processed by the attached computer system.

2.3.3 Fourier-transform infrared (FTIR) spectrometry

Perkin Elmer FTIR spectrometer was used to determine functional groups in RAL, ALB and CAL as described in earlier study [8].

2.3.4 Scanning electron microscopy–energy-dispersive X-ray spectrometry (SEM–EDX)

SEM (XL 20 Philips) attached with Energy-dispersive X-ray (SEM–EDX) was utilized to examine surface morphology and elemental composition of RAL, ALB and CAL.

2.3.5 N_2 adsorption–desorption isotherms

Pore size distribution, volume and specific surface areas of RAL, ALB and CAL were determined using programmed gas adsorption analyzer (Quanta Chrome Instruments, USA) with N_2 adsorption–desorption isotherms at -196 °C.

2.3.6 X-ray diffractometry

X-ray diffraction analyzer (Rigaku Dmax 7000) was used to investigate the structure of RAL, ALB and CAL. The adsorbents were scanned at diffraction angle (2θ) operated between 10° and 80° with scanning speed of 3°/min.

2.3.7 pH profile studies

Each of the adsorbents (40 mg) was weighed separately into different conical flasks (100 mL each) containing aliquot (25 mL of 100 mg/L) of prepared BPB dye solution. HCl (0.1 M) and NaOH (0.1 M) were used to adjust pH value of the BPB dye solutions from pH 1–13. Each of BPB dye solutions containing adsorbent was stirred for 60 min at 301 K and 100 rpm. Initial (before adsorption) and final (after adsorption) pH values of the BPB dye were noted and recorded as pH_i and pH_f , respectively. The difference between pH_i and pH_f was recorded as change in pH (ΔpH) value. Point of intersection of the graph of ΔpH against pH_i at which pH values of BPB–RAL, BPB–ALB and BPB–CAL adsorption systems were zero indicated zero point charge (pH_{PZC}) of the adsorbents' surfaces.

2.3.8 Adsorption experiments

BPB dye sequestration from aqueous solutions was investigated using RAL, ALB and CAL as adsorbents. The quantity of BPB in solution before and after the adsorption process was determined as described by Jabar and Odusote [8]. Optimum percentage BPB dye (Eq. 2) removed from aqueous solution was evaluated using constant adsorbent dose (40 mg/25 mL), dye initial concentration (100 mg/L), contact time (60 min), pH (3), volume (25 mL), temperature (301 K) and agitation speed (100 rpm) of dye solution in conical flask (100 mL).

$$R(\%) = \left(\frac{C_b - C_a}{C_b} \right) \times 100 \quad (2)$$

Effects of BPB dye initial concentration and adsorbent dose on batch adsorption were examined by varying initial concentration from 25 to 125 mg/L and adsorbent dose from 0.01 to 0.05 g/25 mL, respectively. While effects of contact time and temperature on BPB dye adsorption from aqueous solution were carried out by varying time of adsorption from 15 to 75 min and temperature from 303 to 343 K, respectively, keeping other parameters steady as used in optimum BPB dye removal. BPB dye-uptake (mg/g) of each of the adsorbents [28] was calculated as shown in the following equation:

$$q_e = \left(\frac{C_b - C_a}{W} \right) \times V \quad (3)$$

where R (%) and q_e (mg/g) are percentage removal and equilibrium uptake respectively, of BPB dye from aqueous solution using RAL, ALC and CAL as adsorbents. C_b (mg/L) and C_a (mg/L) are BPB dye concentrations before and after adsorption process. W (g) is weight of each of the adsorbents and volume of BPB dye solution is V (L).

After each of the batch adsorption processes, each of the adsorbents was separated from BPB dye solutions, the absorbance (at 580 nm) of the effluents and interpolated concentrations were determined as described by Jabar and Odusote [8].

2.3.9 Adsorption models

Information acquired from effects of adsorbent dose, contact time and temperature on BPB dye removal from aqueous solution were used to evaluate isotherm (Freundlich and Langmuir), kinetic (pseudo-first and -second order) and thermodynamic (van't Hoff) models, respectively. Details of adsorption models and their equations were described in previous study [28].

3 Results and discussion

3.1 Physicochemical and thermal analysis of the adsorbents

The results presented in Table 1 show that the pH and VM (organic) decreased after carbonization and chemical activation of RAL and ALB, respectively. Decrease in value of pH of RAL from ≈ 9 to ≈ 8 and ≈ 7 after carbonization and activation, respectively, was in agreement with Bello et al. [36] and Ahmedna et al. [37]. Decrease in value of

VM after processing might be as a result of evaporation of part of organic matter during pyrolysis and leaching out of part of inorganic matters during chemical activation [38]. In contrary, progressive increase in MC, IN and FC of the sample was noticed as RAL was pyrolyzed and chemically activated. MC and IN are measured of adsorption of moisture from atmosphere and iodine from solution, respectively, by the adsorbents. Increase in MC and IN might be as a result of thermal decomposition of RAL to form porous carbonaceous material (ALB) with enhanced adsorption capacity and CAL with more enhanced adsorption capacity due to discharge of inorganic matters from the surface of adsorbent after acid activation. According to Ekpete and Horsfall [39], IN value of ALB and CAL > 100 was associated with their mesoporous structure and that of RAL < 100 was associated with its microporous structure [40]. Therefore, it can be said that CAL might have the best adsorption capacity, followed by ALB according to Adowei et al. [40]. The higher FC of ALB and CAL was an indication of better adsorption capacity of processed AL adsorbents according to Bello et al. [36]. The increase in AC of RAL after pyrolysis might be as a result of evaporation and degradation of some volatile and organic components, respectively, in the adsorbent and decrease in AC of CAL after chemical activation of ALB might be due to possibility of leached out of part of ALB's inorganic components during chemical activation [36].

The results of thermogravimetric analysis of RAL, ALB and CAL are shown in Fig. 1a. The thermogravimetric profiles of the adsorbents were characterized by four degradation stages. The first degradation stage was between 30 and 125.3 °C indicating evaporation of water with 4.06, 8.03 and 9.16% corresponding weight loss in RAL, ALB and CAL, respectively, according to Ahmad and Alrozi [41]. The second degradation stage could be attributed to degradation of pectin and part of hemicellulose; it occurred in the temperature range 125.3–193.2 °C with the corresponding weight loss of 2.0% in RAL and no weight loss in ALB and CAL. This indicated that ALB and CAL contained neither pectin nor hemicellulose. Weight loss in the third degradation stage could be associated to degradation of light volatile matters [33]. These organic matters decomposed at temperature range between 125.3 and 254.7 °C corresponding to 47.33, 9.82 and 7.20% weight loss in RAL, ALB and CAL, respectively [42]. The last degradation stage witnessed weight loss 41.73, 71.73 and 83.46% in RAL, ALB and CAL at temperature between 254.7 and 920 °C. This might be due to degradation of denser volatile matters [38, 42]. Above 920 °C, the weight of residual matters remained constant and regarded as weight of inorganic matters in the adsorbents [23]. These observations are in accordance to the findings of Ali et al. [38].

Table 1 Properties of RAL, ALB and CAL

Properties	RAL	ALB	CAL
Moisture content (%)	4.06	8.03	9.16
Volatile matters (%)	72.09	15.64	10.29
Fixed carbon (%)	19.02	66.05	73.31
Ash content (%)	4.83	10.28	7.24
Iodine number	44.32	102.64	218.22
pH	9.03	7.97	6.92
S_{BET} (cm ² /g)	327	609	785
D_p (nm)	1.82	2.03	2.09
V_{total} (cm ³ /g)	0.46	0.52	0.58

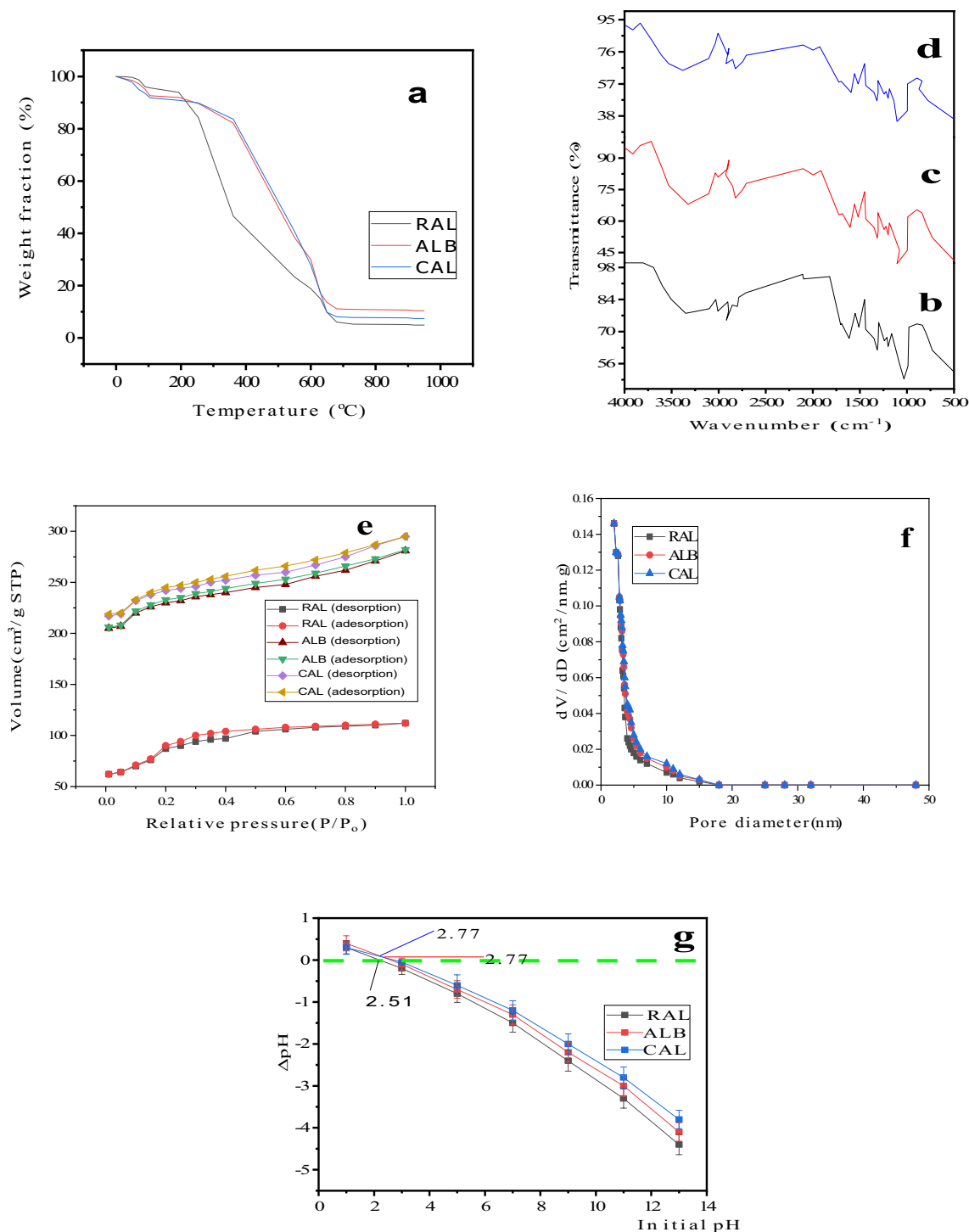


Fig. 1 a TGA thermograms, b–d FTIR spectra, e N₂ adsorption–desorption isotherms, f pore size distributions and g Zero potential charges (pHpzc) of RAL, ALB and CAL adsorbents

3.2 Fourier transform infrared spectrometry

Figure 1b–d depicts effect of processing on functional group characteristics of RAL, ALB and CAL. Broad peak at 3350.2 cm⁻¹ in Fig. 1b is a characteristic feature of adsorbed

water molecule and/or alcoholic –OH functional group in RAL [33, 43]. The broad nature of this peak was enhanced in ALB and CAL (Fig. 1c, d), probably due to increase in moisture absorptivity of the adsorbents. Stretching peaks between 2918.5 and 2851.4 cm⁻¹ indicated presence of –CH

bond, which was a saturated aliphatic moiety of hemicellulose and cellulose in prepared adsorbents [44]. Shift in $-\text{CH}$ peak noticed in ALB and CAL might be as a result of release of hydrogen molecules from RAL during carbonization and acid activation. Peak due to $-\text{C}=\text{O}$ appeared at 1703.4 cm^{-1} indicating presence of carbonyl functional group of hemicellulose and lignin in RAL [45]. There was a peak reduction in treated almond leaf samples (ALB and CAL). The peak observed at 1613.9 cm^{-1} corresponded to the secondary amine ($-\text{NH}$) group in RAL. This functional group was equally noticed in ALB and CAL [8]. $-\text{CH}_3$ and $-\text{CH}$ were symmetric bending of organic compound observed between 1438.8 and 1315.8 cm^{-1} in the adsorbents [46]. The stretching vibrations at 1200.2 cm^{-1} and 1032.5 cm^{-1} confirmed $-\text{OH}$ functional group of adsorbed moisture and $\text{C}-\text{O}$ stretching of organic component, respectively, in RAL, ALB and CAL [47].

3.3 Scanning electron microscopy–energy-dispersive X-ray spectrometry (SEM–EDX)

SEM–EDX results of RAL, ALB and CAL are presented in Fig. S1a–f. The surface morphology of the prepared adsorbents was rough with irregular shapes and several pores. These attributes predicted possibility of the prepared adsorbents to possess good adsorption capacities for removal of pollutants (dye molecules, heavy metals, organic matters, etc.) from wastewater according to Regti et al. [48]. Thermal degradation of RAL (lignocellulose) during pyrolysis converted it to ALB with well-developed surface area and active sites (pores) (Fig. S1b). Acid activation of ALB enhanced surface area and porosity of the adsorbent due to hydrolysis of organic matters and leaching out of inorganic matters to form CAL (Fig. S1c). EDX spectra of RAL, ALB and CAL presented in Fig. S1d–f show characteristic lines which are proportional to the corresponding elements in each of the adsorbents. Carbon and oxygen were two major elements detected in RAL, ALB and CAL. The adsorbents have high amount of carbon and low amount of oxygen.

3.4 N_2 adsorption–desorption isotherms

Figure 1e, f shows N_2 adsorption–desorption curves and pore size distributions of RAL, ALB and CAL at $-196\text{ }^\circ\text{C}$. The N_2 adsorption–desorption curve of RAL displayed Type II adsorption isotherm, while those of ALB and CAL corresponded to the Type IV adsorption isotherms. The surface areas of RAL, ALB and CAL were high, estimated average pore diameter of RAL was less than 2 and those of ALB and CAL were greater than 2 (Table 1). According to Shi et al. [49], adsorbent diameter was defined by IUPAC as mesopore if its within 2 and 50 nm, micropore if its < 2 nm and macropore if its > 50 nm.

Based on these results, it can be said that pyrolysis and acid activation of RAL widen pore diameter from micropore to mesopore surface structure.

3.5 XRD analysis of RAL, ALB and CAL

XRD diffraction patterns of RAL, ALB and CAL are shown in Fig. S2a–c. The diffractograms of the adsorbents show several peaks with prominent peak of amorphous curve observed at $2\Theta = 20.9^\circ$ in RAL [50]. Other diffraction patterns in RAL are $2\Theta = 9.4^\circ, 29.2^\circ, 32.1^\circ, 36.8^\circ, 41.3^\circ, 45.2^\circ, 49.1^\circ$ and 51.5° . After pyrolysis of RAL and chemical activation of ALB, emergent of new diffraction peaks at $2\Theta = 25.6^\circ$ in ALB and $2\Theta = 24.9^\circ$ in CAL were an indication of amorphous carbon according to Ali et al. [47]; Pang et al. [51]. Also, slight shift in other diffraction peaks occurred after pyrolysis of RAL and acid activation of ALB. These observations authenticated the real images (photographs) of AL, RAL, ALB and CAL shown in Fig. S2d–g.

3.6 Zero potential charges (pHpzc)

Points at which surfaces of RAL, ALB and CAL (prepared adsorbents) have zero potential charges (pHpzc) are shown in Fig. 1g. The surfaces of the adsorbents were predominantly cationic charged at $\text{pH} < 3$ and anionic charged at $\text{pH} > 3$ in BPB dye solution. These observations indicated possibility of electrostatic attraction between cationic surfaces charged adsorbents and anionic charged BPB dye at $\text{pH} < \text{pHpzc}$. In contrary, there might be electrostatic repulsion between adsorbents and anionic charged BPB dye at $\text{pH} > \text{pHpzc}$, because at any $\text{pH} > 3$, surfaces of all the adsorbents were negatively charged. Therefore, sequestration of BPB dye from aqueous solution might be better at $\text{pH} \leq 3$ than $\text{pH} > 3$ due to electrostatic effect. These observations agreed with Thue et al. [30]. Although, electrostatic force might not be only force of adsorption of BPB dye onto prepared adsorbents from aqueous solution, others might be mechanical, van der Waals and π/π interaction [52].

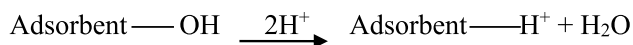
3.7 BPB dye adsorption mechanism onto prepared adsorbents

pH is a key parameter for sequestration of BPB dye from contaminated water. In water, BPB dye ionizes to form BPB dye anionic specie and cationic sodium (Scheme 1).

At pH below pHpzc of the prepared adsorbents, they acquired positively charged surfaces (Scheme 2).



Scheme 1 Ionization of BPB dye in solution



Scheme 2 Ionic charge on adsorbent surface at $\text{pH} < \text{pHpzc}$

Consequently, there exists strong electrostatic attraction of negatively charged BPB dye molecule to positively charged adsorbents (Scheme 3), resulting into optimum dye removal [53].

Although, percentage BPB dye adsorbed from solution at $\text{pH} 1$ is slightly lower than that of $\text{pH} 3$ (Fig. 2a). This might be consequence of competition between positively charged adsorbents surface sites and H^+ of strong acidic medium for BPB dye in solution at $\text{pH} 1$ according to Zeroual et al. [54].

Contrarily, when pH of the dye solution increased above pHpzc of the adsorbents, surfaces of the adsorbents became negatively charged (Scheme 4) and quantity of BPB dye uptake onto the adsorbents' surfaces decreased (Fig. 2a). This is an indication of electrostatic repulsion between negatively charged adsorbents and BPB dye (Scheme 3) according to Zhou et al. [55]. Dye-uptake followed the same trend (Fig. 2b).

3.8 Adsorption experiments

Percentage BPB dye adsorbed onto RAL, ALB and CAL decreased slightly as dye initial concentration increased from 25 to 100 mg/L . A noticeable reduction in quantity of BPB dye adsorbed was notice at initial concentration 125 mg/L (Fig. 2c). This is an indication of possibility of saturation of the adsorbents' adsorption sites at initial dye concentration of 100 mg/L , which led to a noticeable reduction in percentage adsorption at slight increase in initial concentration. Although, increase in dye-uptake was noticed as initial concentration increased from 25 to 125 mg/L (Fig. 2d) as a result of enhancement in rate of collision between molecules of BPB dye in solution and adsorbents. This observation agreed with previous study [8].

Quantity of BPB dye removed from solution improved as adsorbent dose increased from 0.01 to 0.04 $\text{g}/25 \text{ mL}$ (Fig. 2e). This observation was due to increase in dye adsorption sites on the surfaces of adsorbents as adsorbent dose increased. Inconsequential increase in percentage BPB dye removed from solution noticed as adsorbent dose increased from 0.04 to 0.05 $\text{g}/25 \text{ mL}$ might be due to decrease in rate of diffusion of BPB dye from solution onto the adsorbents [8]. Contrarily, dye-uptake reduced as adsorbent dose increased (Fig. 2f). These observations are in line with Boulaiche et al. [56].

The dye-uptake and percentage BPB dye adsorbed from solution increased rapidly up to 60 min adsorption time, indicating 60 min as equilibrium time of adsorption process. Thereafter, there was an insignificant increase in dye-uptake and percentage dye removed from aqueous solution (Fig. 2g, h). Probability of adsorbents' active sites exhaustion as contact time increased up to 60 min might responsible for this observation according to Jabar et al. [29].

Temperature has a little influence on dye-uptake and percentage BPB dye adsorbed onto the prepared adsorbents as shown in Fig. 2i, j. Although, there was a slight reduction in dye-uptake and percentage dye removed as adsorption temperature increased from 301 to 343 K.

3.9 Adsorption models

The commonly used models for optimizing design of adsorption system are isotherm, kinetic and thermodynamic model. These models give adequate insight of affinity of dye for a unit mass of adsorbent at a particular temperature within a given time.

3.9.1 Adsorption isotherm

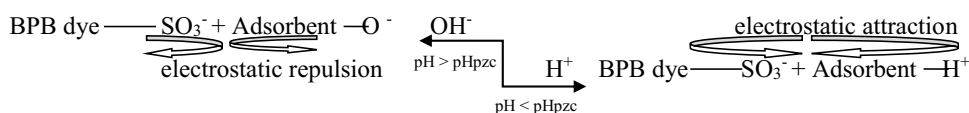
Maximum monolayer adsorption capacities of RAL, ALB and CAL adsorbents for removing BPB dye from aqueous solution were estimated using Langmuir model (Eq. 4) which assumes monolayer coverage of dye onto adsorbent surface of similar active sites and energy of adsorption [5].

$$\frac{1}{q_e} = \frac{1}{Q_{\max} K_L} \left(\frac{1}{C_a} \right) + \frac{1}{Q_{\max}} \quad (4)$$

where Q_{\max} is maximum monolayer adsorption capacity (mg/g), K_L is Langmuir isotherm constant correlated to energy of adsorption and affinity of the binding sites of adsorbent for dye (L/mg).

Q_{\max} and K_L of the adsorbents were acquired, respectively, from intercept and slope of plot of $\frac{1}{q_e}$ against $\frac{1}{C_a}$ (Fig. 3a). Q_{\max} of CAL was almost as double as that of RAL and Q_{\max} of ALB was next to that of CAL. Contrarily, energy required for adsorption of BPB dye onto RAL was virtually double that of CAL (Table 2). This indicated that carbonaceous materials are more active than lignocellulosic material for sequestering of BPB dye from aqueous solution. R_L , which is defined as dimensionless separation faction that determines nature of adsorption process of Langmuir isotherm was calculated from

Scheme 3 Electrostatic effect on adsorption of BPB dye onto prepared adsorbent



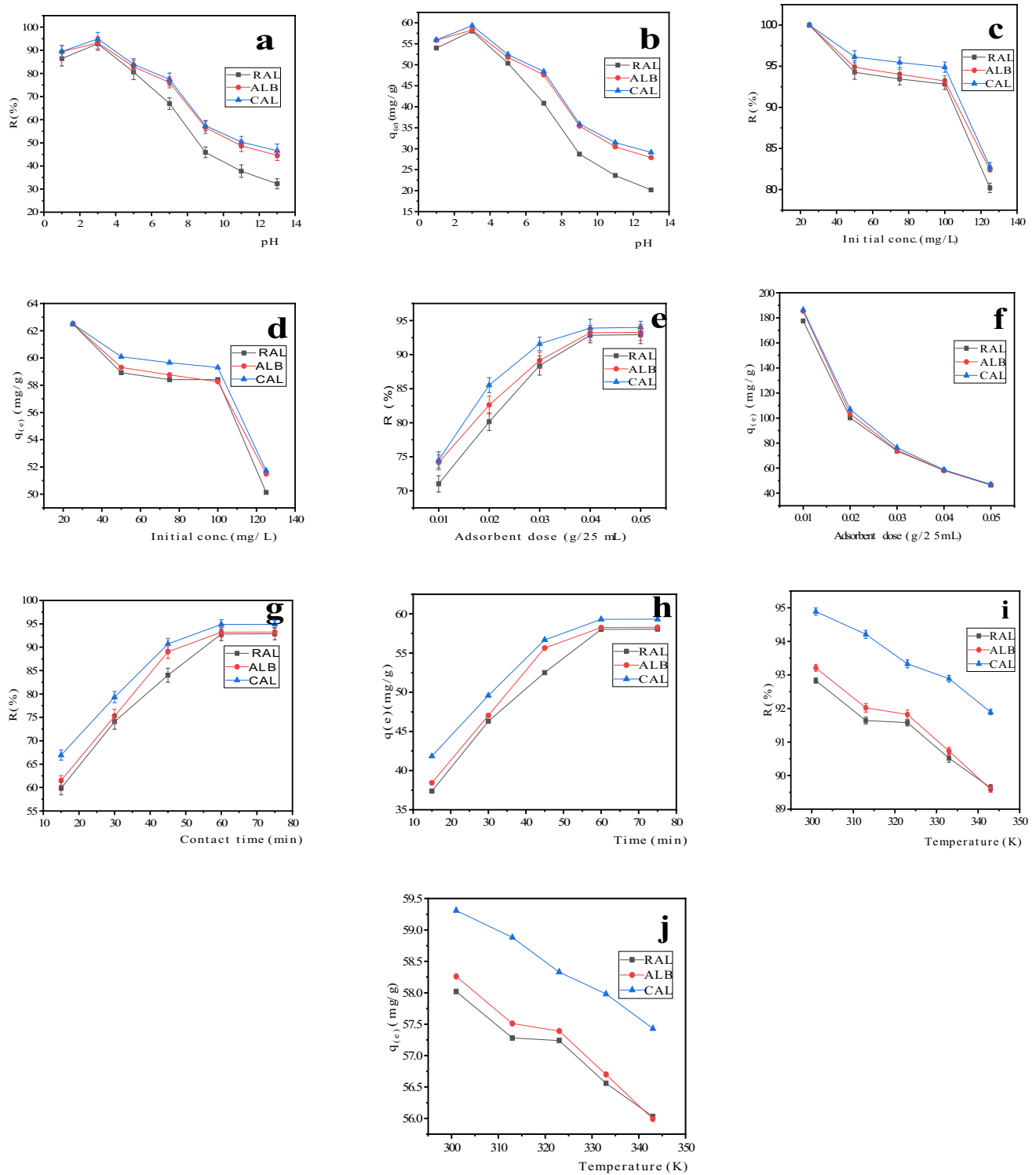
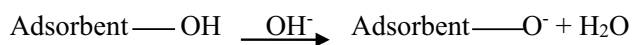


Fig. 2 Adsorption of BPB dye on RAL, ALB and CAL adsorbents **a, b** effect of pH, **c, d** effect of initial concentration, **e, f** effect of adsorbent dose, **g, h** effect of contact time, and **i, j** effect of temperature



Scheme 4 Ionic charge on adsorbent surface at $\text{pH} > \text{pH}_{\text{pzc}}$

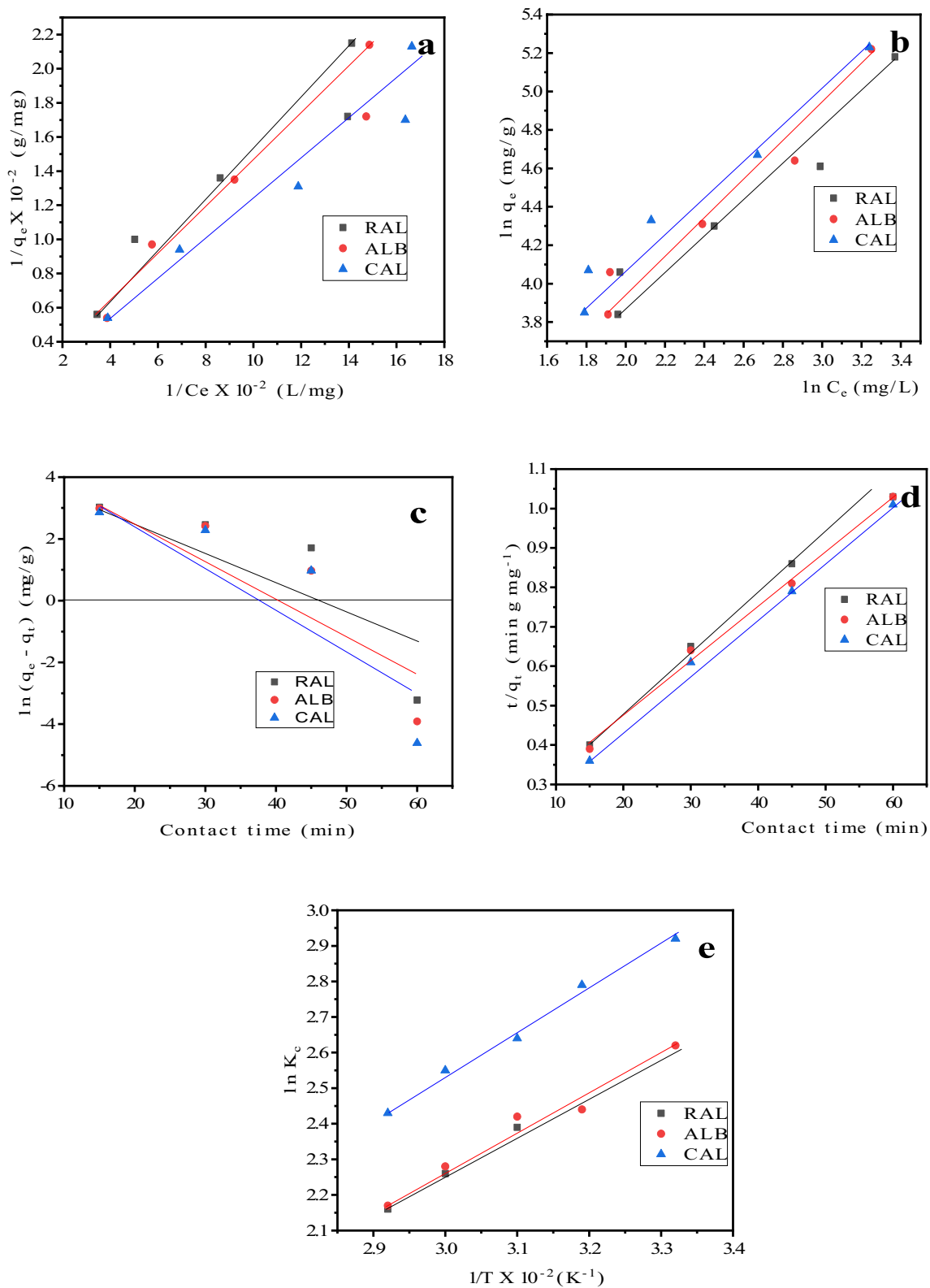


Fig. 3 BPB dye Adsorption models on RAL, ALB and CAL adsorbents **a** Langmuir isotherm, **b** Freundlich isotherm, **c** Pseudo-first order kinetic, **d** Pseudo-second order kinetic, and **e** van't Hoff thermodynamic model

Table 2 Isotherm parameters for BPB–RAL, BPB–ALB and BPB–CAL adsorption process

Adsorption process	Langmuir				Freundlich			
	Q_{\max} (mg/g)	K_L (L/mg)	R_L	R^2	K_F (mg/g [L/mg] ^{1/n})	$\frac{1}{n}$	n	R^2
BPB–RAL	365.36	0.023	0.30	0.9218	10.23	0.81	1.23	0.9462
BPB–ALB	535.62	0.016	0.38	0.9308	9.03	0.90	1.11	0.9553
BPB–CAL	730.46	0.013	0.43	0.9392	11.32	0.86	1.16	0.9751

Eq. 5 to be highest in CAL and lowest in RAL (Table 5). These results authenticated those obtained for Q_{\max} and K_L .

$$R_L = \frac{1}{(1 + K_L C_b)} \quad (5)$$

Adsorption of BPB dye onto RAL, ALB and CAL was favorable since $0 < R_L < 1$ according to Adetuyi and Jabar [28].

Freundlich isotherm proposes that multilayer adsorption of dye occurs onto the adsorbent (solid) heterogeneous surface with non-uniform active sites [53]. The linear relationship between dye concentration at equilibrium and adsorption capacity is given in Eq. 6.

$$\ln q_e = \frac{1}{n} \ln C_a + \ln K_F \quad (6)$$

where n and K_F (mg/g [L/mg]^{1/n}) are adsorption intensity and capacity, respectively, obtained from intercept and slope of linear plot of $\ln q_e$ against $\ln C_a$ (Fig. 3b). The values of $\frac{1}{n}$ greater than zero and less than one ($0 < \frac{1}{n} < 1$) indicated favorability of adsorption of BPB onto RAL, ALB and CAL adsorbents (Table 2) [57].

Although, sequestration of BPB dye from solution onto the prepared adsorbents was favorable for both Langmuir and Freundlich isotherms, but isotherm was better fit with Freundlich than Langmuir due to higher correlation coefficient (R^2) of Freundlich model (Table 2).

3.9.2 Adsorption kinetics

Investigation on rate of adsorption is a basic requirement for designing a fast and functional model [46]. The suitable

order of rate constant for effective design of adsorption plant can be determined from pseudo-first and -second-order kinetic [53]. The expression of pseudo-first-order is given in the following equation:

$$\ln(q_e - q_t) = \ln q_e - k_1(t) \quad (7)$$

Pseudo-second-order kinetic can be used to describe adsorption capacity for all dye concentrations and forecast nature of the adsorption process (either physisorption or chemisorption) [57]. The linearized pseudo-second order equation is expressed as in the following equation:

$$\frac{t}{q_t} = \frac{1}{k_2 q_e^2} + \frac{1}{q_e}(t) \quad (8)$$

where q_e and q_t are dye-uptake (mg/g) at equilibrium and at time t (min), respectively, k_1 (min⁻¹) and k_2 (g mg⁻¹ min⁻¹) are rate constants of pseudo-first and -second-order kinetic, respectively. Pseudo-second-order initial rate of adsorption h_2 (mg g⁻¹ min⁻¹) is expressed as shown in the following equation:

$$h_2 = k_2 q_e^2 \quad (9)$$

The values of k_1 and q_e were determined from slope and intercept of graph of $\ln(q_e - q_t)$ versus t (Fig. 3c) in pseudo-first-order kinetic, while values q_e and k_2 of pseudo-second-order kinetic were obtained from slope and intercept of plot of $\frac{t}{q_t}$ against t (Fig. 3d). Table 3 shows adsorption kinetic parameters for adsorption of BPB dye onto RAL, ALB and CAL. It was observed from Table 3 that rate constants of the kinetic study increased from adsorption system of raw (BPB–RAL) to pyrolyzed biochar (BPB–ALB) and to chemically activated carbon (BPB–CAL), indicating adsorption process to be faster

Table 3 Kinetic parameters for BPB–RAL, BPB–ALB and BPB–CAL adsorption process

Adsorption process	Pseudo-first order			Experimented value $q_{e(\text{exp})}$ (mg/g)	Pseudo-second order			
	$q_{e(\text{cal})}$ (mg/g)	K_1 (min ⁻¹)	R^2		$q_{e(\text{cal})}$ (mg/g)	h_2	$K_2 \times 10^{-4}$ (mg g ⁻¹ min ⁻¹)	R^2
BPB–RAL	354.29	0.13	0.7740	92.89	71.43	4.76	9.33	0.9928
BPB–ALB	471.07	0.15	0.8316	93.24	71.94	5.13	9.91	0.9951
BPB–CAL	547.30	0.16	0.8036	94.91	70.43	6.25	12.60	0.9964

as the adsorbents are being processed. Significant difference between pseudo-first order estimated values ($q_{e(cal)}$) and experimental values ($q_{e(exp)}$) showed that adsorption of BPB dye onto RAL, ALB and CAL did not fit with pseudo-first-order model. In contrary, estimated values ($q_{e(cal)}$) closer to experimental values ($q_{e(exp)}$) pointed out that adsorption process was better fit with pseudo-second order model. Higher correlation coefficient (R^2) of pseudo-second order model than pseudo-first-order model in all the adsorption system (Table 3) confirmed suitability of pseudo-second order model to all adsorption system. These observations are in line with our previous study [57].

3.9.3 Adsorption thermodynamics

Adsorption thermodynamic predicts relationship between adsorption temperature and capacity. Enthalpy change (ΔH) and entropy change (ΔS) were thermodynamic parameters of adsorption of BPB dye onto RAL, ALB and CAL evaluated from slopes and intercepts of van't Hoff plot of $\ln K_c$ against $\frac{1}{T}$ (Fig. 3e) obtained from thermodynamic equation (Eq. 10) and presented in Table 4. The free energy change (ΔG) of adsorption system was obtained from Eqs. 11 and 12.

$$\ln K_c = \frac{\Delta S}{R} - \frac{\Delta H}{R} \left(\frac{1}{T} \right) \tag{10}$$

$$\Delta G = -RT \ln K_c \tag{11}$$

$$\Delta G = \Delta H - T\Delta S \tag{12}$$

The negative values of ΔH throughout the adsorption processes showed the exothermic nature of the processes. The negative values and decrease in magnitudes of ΔG as adsorption temperature increased indicated that adsorption process was spontaneous and less favorable as temperature increased [53]. Negative values of ΔS designated an enhanced randomness at the BPB-adsorbent interface as sequestration process progressed according to El-Gamal et al. [6]; You et al. [58]. Reduction in values of ΔS from BPB-RAL to BPB-CAL dye-adsorbent system pointed out reduction in degree of mobility (randomness) of dye molecules off surfaces of BPB dye adsorbed adsorbents [58].

3.9.4 Comparison of adsorption capacities of RAL, ALB and CAL with other adsorbents

Maximum monolayer adsorption capacities (Q_{max}) of RAL, ALB, CAL and those of other adsorbents reported in the literature for adsorption of dye from aqueous solution are shown in Table 5. RAL, ALB and CAL's Q_{max} are more than thirty, twenty and ten times higher than those of adsorbents derived from polymer-clay composite [5], sorrel's cement nanoparticles [6], mesoporous hybrid gel [58] and α -Chitin

Table 4 Thermodynamic parameters for BPB-RAL, BPB-ALB and BPB-CAL adsorption process

Adsorption process	ΔH (kJ mol ⁻¹)	ΔS_L (J mol ⁻¹ K ⁻¹)	ΔG (kJ mol ⁻¹)				
			301 K	313 K	323 K	333 K	343 K
BPB-RAL	- 7.83	- 14.73	- 3.39	- 3.22	- 3.07	- 2.92	- 2.78
BPB-ALB	- 8.91	- 21.36	- 2.48	- 2.23	- 2.01	- 1.80	- 1.59
BPB-CAL	- 10.20	- 26.12	- 2.34	- 2.02	- 1.76	- 1.50	- 1.24

Table 5 Comparison of adsorption capacities of RAL, ALB and CAL with other adsorbents for dye removal from aqueous solution

Adsorbent	Dye	Q_{max} (mg g ⁻¹)	References
Polymer-clay composite	BPB	10.78	[5]
Sorel's cement nanoparticles	BPB	16.39	[6]
<i>Rhizopus stolonifer</i> biomass	BPB	769.00	[54]
Mesoporous hybrid gel	BPB	27.50	[58]
α -Chitin nanoparticles	BPB	22.72	[59]
CuS-Activated carbon nanoparticle	BPB	106.40	[60]
Almond shell	Eriochrome black T	123.92	[61]
Almond shell	Malachite dye	126.90	[61]
Almond peel	Brilliant green dye	30.00	[62]
Almond peel	Brilliant green industrial effluent	17.00	[62]
RAL	BPB	365.36	This study
ALB	BPB	535.62	This study
CAL	BPB	730.46	This study

nanoparticles [59], respectively. Equally, AL-derived adsorbents' Q_{\max} are more than three, five and twenty four times higher than those of CuS-activated carbon nanoparticle [60], almond shell [61] and almond peel [62], respectively. Although, it was observed that CAL has virtually equal Q_{\max} as that of *Rhizopus stolonifer* biomass [54], but it can be said that AL-derived adsorbents can compete favorably with those adsorbents reported in the literature for removal of BPB dye from aqueous solution.

4 Conclusion

The prepared biomaterials (RAL, ALB and CAL) were successfully used as novel, low-cost and eco-friendly alternative adsorbents for sequestration of hazardous BPB dye from aqueous solution with excellent adsorption potential for removing more than 90% of BPB dye. Adsorption capacities of the prepared adsorbents were established to be significantly better than others reported for removal dye from aqueous solution.

The adsorption data showed good fit to Freundlich isotherm and pseudo-second order kinetic models, while thermodynamics study indicated adsorption process to be spontaneous and exothermic.

Therefore, these prepared adsorbents and adsorption models used can be recommended for industrial scale treatment of any wastewater polluted with dye of any class.

Acknowledgements The authors appreciate Dr. Mathew A. Adabayo of Chemistry Department, FUTA for his efforts on the success of this research work.

Compliance with ethical standards

Conflict of interest On behalf of all authors, the corresponding author states that there is no conflict of interest.

References

- Al-Shaalan NH, Ali I, AlOthman ZA, Al-Wahaibi LH, Alabdulmonem H (2019) High performance removal and simulation studies of diuron pesticide in water on MWCNTs. *J Mol Liq* 289:111039. <https://doi.org/10.1016/j.molliq.2019.111039>
- Kumar PS, Saravanan A, Rajan PS, Yashwanthraj M (2016) Nanoscale zero-valent iron-mpregnated agricultural waste as an effective biosorbent for the removal of heavy metal ions from wastewater. *Text Cloth Sust* 2:3. <https://doi.org/10.1186/s40689-016-0014-5>
- Jabar JM, Ogunmokin AI, Taleat TAA (2020) Color and fastness properties of mordanted *Bridelia ferruginea* B dyed cellulosic fabric. *Fash Text* 7:1. <https://doi.org/10.1186/s40691-019-0195-z>
- Ali I, Alharbi OML, Allothman ZA, Badjah AY, Alwarthan A, Basheer AA (2018) Artificial neural network modelling of amido black dye sorption on iron composite nano material: Kinetics and thermodynamics studies. *J Mol Liq* 250:1–8. <https://doi.org/10.1016/j.molliq.2017.11.163>
- El-Zahhar AA, Awwad NS, El-Katori EE (2014) Removal of bromophenol blue dye from industrial waste water by synthesizing polymer-clay composite. *J Mol Liq*. <https://doi.org/10.1016/j.molliq.2014.07.034>
- El-Gamal SMA, Amin MS, Ahmed MA (2015) Removal of methyl orange and bromophenol blue dyes from aqueous solution using Sorel's cement nanoparticles. *J Environ Chem Eng* 3:1702–1712. <https://doi.org/10.1016/j.jece.2015.06.022>
- Sartape AS, Mandhare AM, Jadhav VV, Raut PD, Anuse MA, Kolekar SS (2014) Removal of malachite green dye from aqueous solution with adsorption technique using *Limonia acidissima* (wood apple) shell as low cost adsorbent. *Arab J Chem*. <https://doi.org/10.1016/j.arabjc.2013.12.019>
- Jabar JM, Odusote YA (2020) Removal of cibacron blue 3G-A (CB) dye from aqueous solution using chemo-physically activated biochar from oil palm empty fruit bunch fiber. *Arab J Chem* 13:5417–5429. <https://doi.org/10.1016/j.arabjc.2020.03.020>
- Abebe B, Murthy HCA, Dessie Y (2020) Synthesis and characterization of Ti-Fe oxide nanomaterials: adsorption-degradation of methyl orange dye. *Arab J Sci Eng*. <https://doi.org/10.1007/s13369-019-04328-1>
- Mohan N, Balasubramanian N, Basha CA (2007) Electrochemical oxidation of textile wastewater and its reuse. *J Hazard Mater* 147:644–651
- Malana MA, Parveen S, Qureshi RB (2016) Adsorptive removal of organic dyes from aqueous solutions using acrylic acid–acrylonitrile–Nisopropylacrylamide polymeric gels as adsorbents: linear and non linear isotherms. *Desalin Water Treat*. <https://doi.org/10.1080/19443994.2015.1132393>
- Ashtoukhy E, El SZ (2009) Loofa egyptiaca as a novel adsorbent for removal of direct blue dye from aqueous solution. *J Environ Manage* 90:2755
- Daneshvar N, Ayazloo M, Khataee AR, Pourhassan M (2007) Biological decolorization of dye solution containing malachite green by microalgae *Cosmarium* sp. *Bioresour Technol* 98:1176–1182
- Chiou MS, Ho PY, Li HY (2004) Adsorption of anionic dyes in acid solutions using chemically cross-linked chitosan beads. *J Dyes Pigms* 60:69–84
- Nitzsche R, Gröngroft A, Kraume M (2011) Separation of lignin from beech wood hydrolysate using polymeric resins and zeolites—determination and application of adsorption isotherms. *Sep Purif Technol* 83:50–56. <https://doi.org/10.1016/j.seppur.2018.07.077>
- Adetuyi AO, Mojibola AA, Jabar JM (2013) Thermo-kinetics studies of indigo dye effluent removal with kaolin from *Tectona grandis* and indigo dye effluents. *Pak J Sci Ind Ser A Phys Sci* 56(2):93–99
- Elhami NPSH (2010) Removal of malachite green from water samples by cloud point extraction using Triton X-100 as non-ionic surfactant. *Environ Chem Lett* 8:53
- Forgacs E, Cserha'ti T, Oros G (2004) Removal of synthetic dyes from wastewaters: a review. *Environ Int* 30:953–971
- Wu K, Xie Y, Zhao J, Hidaka H (1999) Photo-Fenton degradation of a dye under visible light irradiation. *J Mol Catal A Chem* 144:77–84
- Robinson T, McMullan G, Marchant R, Nigam P (2001) Remediation of dyes in textile effluent: a critical review on current treatment technologies with a proposed alternative. *Bioresour Technol* 77:247–255
- Mittal J, Jhare D, Vardhan H, Mittal A (2014) Utilization of bottom ash as a low-cost sorbent for the removal and recovery of a toxic halogen containing dye eosin yellow. *Desalin Water Treat* 52:4508–4519

22. Agarwal M, Singh K (2017) Heavy metal removal from wastewater using various adsorbents: a review. *J Water Reuse Desalin* 7(4):387–419
23. Vandevivere PC, Bianchi R, Verstraete W (1998) Treatment and reuse of wastewater from the textile wet-processing industry: review of emerging technologies. *J Chem Technol Biotechnol* 72:289–302
24. Al-Rashed SM, Al-Gaid AA (2012) Kinetic and thermodynamic studies on the adsorption behavior of Rhodamine B dye on Duolite C-20 resin. *J Saudi Chem Soc* 16:209–215. <https://doi.org/10.1016/j.jscs.2011.01.002>
25. Al-Degs YS, El-Barghouthi MI, El-Sheikh AH, Walker GM (2008) Effect of solution pH, ionic strength, and temperature on adsorption behavior of reactive dyes on activated carbon. *Dyes Pigments* 77:16–23
26. Iqbal MJ, Ashiq MN (2007) Adsorption of dyes from aqueous solutions on activated charcoal. *J Hazard Mater* 139:57–66
27. Kasperiski FM, Lima EC, Umpierrez CS, dos Reis GS, Thue PS, Lima DR, Dias SLP, Saucier C, da Costa JB (2018) Production of porous activated carbons from *Caesalpinia ferrea* seed pod wastes: highly efficient removal of captopril from aqueous solutions. *J Clean Prod* 197:919–929
28. Adetuyi AO, Jabar JM (2010) Adsorption isotherm studies of indigo on some activated agro-solid wastes. *Asian dyes* 7(3):46–49
29. Jabar JM, Odusote YA, Alabi KA, Ahmed IB (2020) Kinetics and mechanisms of congo-red dye removal from aqueous solution using activated *Moringa oleifera* seed coat as adsorbent. *Appl Water Sci* 10(6):136. <https://doi.org/10.1007/s13201-020-01221-3>
30. Thue PS, Lima DR, Naushad M, Lima EC, de Albuquerque YRT, Dias SLP, Cunha MR, Dotto GL, de Brum AS (2020) High removal of emerging contaminants from wastewater by activated carbons derived from the shell of cashew of Para. *Carbon Lett.* <https://doi.org/10.1007/s42823-020-00145-x>
31. Esparza G, DeJong TM, Weinbaum SA, Klein I (2001) Effects of irrigation deprivation during the harvest period on yield determinants in mature almond trees. *Tree Physiol* 21:1073–1079
32. Lampinen BD, Tombesi S, Metcalf SG, DeJong TM (2011) Spur behaviour in almond trees: relationships between previous year spur leaf area, fruit bearing and mortality. *Tree Physiol* 31:700–706. <https://doi.org/10.1093/treephys/tpr069>
33. Ozsin G, Kilic M, Apaydin-Varol E, Putun AE (2019) Chemically activated carbon production from agricultural waste of chickpea and its application for heavy metal adsorption: equilibrium, kinetic, and thermodynamic studies. *Appl Water Sci* 9:56. <https://doi.org/10.1007/s13201-019-0942-8>
34. Jabar JM (2016) Effect of chemical modification on physicochemical properties of coir, empty fruit bunch and palm kernel fibres. *Appl Tropical Agric* 2(1):53–158
35. Idowu GA, Fletcher AJ (2019) The manufacture and characterisation of rosid angiosperm-derived biochars applied to water treatment. *BioEnergy Res.* <https://doi.org/10.1007/s12155-019-10074-x>
36. Bello OS, Adegoke KA, Akinyunni OO (2017) Preparation and characterization of a novel adsorbent from *Moringa oleifera* leaf. *Appl Water Sci* 7:1295–1305. <https://doi.org/10.1007/s13201-015-0345-4>
37. Ahmedna M, Marshall WE, Rao RM (2000) Granular activated carbons from agricultural by-products: preparation properties and application in cane sugar refining. *Bull Louisiana State Uni Agric Centre* 54
38. Ali I, Burakov AE, Melezhhik AV, Babkin AV, Burakova IV, Neskornaya MEA, Galunin EV, Tkachev AG, Kuznetsov DV (2019) Removal of copper (ii) and zinc (ii) ions in water on a newly synthesized polyhydroquinone/ graphene nanocomposite material: kinetics, thermodynamics and mechanism. *Chem Select* 4:12708–12718. <https://doi.org/10.1002/slct.201902657>
39. Ekpete OA, Horsfall MJ (2011) Preparation and characterization of activated carbon derived from fluted pumpkin stem waste (*Telfairia occidentalis* Hook F) Res. *J Chem Sci* 1(3):10–17
40. Adowei P, Horsfall JM, Spiff AI (2012) Adsorption of methyl red from aqueous solution by activated carbon produced from cassava (*Manihot esculenta* Cranz) peel waste. *Innov Sci Eng* 2(2):24–33
41. Ahmad MA, Alrozi R (2010) Optimization of preparation conditions for mangosteen peel-based activated carbons for the removal of remazol brilliant blue R using response surface methodology. *Chem Eng J* 165:883–890
42. Hamouz OCSA, Adelabu IO, Saleh TA (2017) Novel cross-linked melamine based polyamine/CNT composites for lead ions removal. *J Environ Manage* 192:163–170. <https://doi.org/10.1016/j.jenvman.2017.01.056>
43. Pang H, Wu Y, Huang S, Ding C, Li S, Wang X, Yu S, Chen Z, Song G, Wang X (2018) Macroscopic and microscopic investigation of uranium elimination by Ca-Mg-Al-layered double hydroxide supported nanoscale zero valent iron. *Inorganic Chem. Frontiers* 5:2657–2665. <https://doi.org/10.1039/C8QI00779A>
44. Pathania D, Sharma S, Singh P (2017) Removal of methylene blue by adsorption onto activated carbon developed from *Ficus carica* bast. *Arab J Chem* 10:S1445–S1451. <https://doi.org/10.1016/j.arabjc.2013.04.021>
45. Bayuo J, Pelig-Ba KB, Abukari MA (2019) Adsorptive removal of chromium (VI) from aqueous solution unto groundnut shell. *Appl Water Sci* 9:107. <https://doi.org/10.1007/s13201-019-0987-8>
46. Etim UJ, Umoren SA, Eduok UM (2016) Coconut coir dust as a low cost adsorbent for the removal of cationic dye from aqueous solution. *J Saudi Chem Soc* 20:S67–S76
47. Ali I, Alharbi OML, ALothman ZA, Alwarthan A, Al-Mohaimed AM (2019) Preparation of a carboxymethylcellulose-iron composite for uptake of atorvastatin in water. *Int J Biol Macromol* 132:244–253. <https://doi.org/10.1016/j.ijbiomac.2019.03.211>
48. Regti A, Laamari MR, Stiriba S, Haddad ME (2017) Removal of basic blue 41 dyes using *Persea americana*-activated carbon prepared by phosphoric acid action. *Int J Ind Chem* 8:187–195
49. Shi J, Zhao Z, Zhou J, Sun T, Liang Z (2019) Enhanced adsorption of As(III) on chemically modified activated carbon fibers. *Appl Water Sci* 9:41. <https://doi.org/10.1007/s13201-019-0919-7>
50. Todorova EV, Chernev GE, Djambazov SP (2014) Structure and properties of functionalized porous silica hybrid materials. *J Inorganic Nonmet Mater* 4:35–43. <https://doi.org/10.4236/ojnm.2014.43006>
51. Pang H, Diao Z, Wang X, Ma Y, Yu S, Zhu H, Chen Z, Hu B, Chen J, Wang X (2019) Adsorptive and reductive removal of U(VI) by *Dictyophora indusiate*-derived biochar supported sulfide NZVI from wastewater. *Chem Eng J* 366:368–377. <https://doi.org/10.1016/j.cej.2019.02.098>
52. Ajayi OA, Okoronkwo AE, Nelcy DSM, Sunday JO (2019) Adsorption of Methylene blue and Congo red from aqueous solution using synthesized alumina–zirconia composite. *Environ Technol.* <https://doi.org/10.1080/09593330.2019.1652696>
53. Banerjee S, Chattopadhyaya MC (2017) Adsorption characteristics for the removal of a toxic dye, tartrazine from aqueous solutions by a low cost agricultural by-product. *Arab J Chem* 10:S1629–S1638. <https://doi.org/10.1016/j.arabjc.2013.06.005>
54. Zeroual Y, Kim BS, Kim CS, Blaghen M, Lee KM (2006) Biosorption of bromophenol blue from aqueous solutions by *Rhizopus stolonifer* biomass. *Water Air Soil Pollu* 177:135–146. <https://doi.org/10.1007/s11270-006-9112-3>
55. Zhou L, Jin J, Liu Z, Liang X, Shang C (2011) Adsorption of acid dyes from aqueous solutions by the ethylenediamine-modified magnetic chitosan nanoparticles. *J Hazard Mater* 185:1045–1052

56. Boulaiche W, Hamdi B, Trari M (2019) Removal of heavy metals by chitin: equilibrium, kinetic and thermodynamic studies. *Appl Water Sci* 9:39
57. Adetuyi AO, Jabar JM (2011) Kinetic and thermodynamic studies of indigo adsorption on some activate bio-solids. *J Chem Soc Pak* 33(2):158–165
58. You L, Wu Z, Kim T, Lee K (2006) Kinetics and thermodynamics of bromophenol blue adsorption by a mesoporous hybrid gel derived from tetra thoxysilane and bis(trimethoxysilyl)hexane. *J Colloid Interface* 300:52–535. <https://doi.org/10.1016/j.jcis.2006.04.039>
59. Dhananasekaran S, Palanivel R, Pappu S (2015) Adsorption of methylene blue, bromophenol blue and coomassie brilliant blue by α -chitin nanoparticles. *J Adv Res*. <https://doi.org/10.1016/j.jare.2015.03.003>
60. Mazaheri H, Ghaedi M, Asfaram A, Hajati S (2016) Performance of CuS nanoparticle loaded on activated carbon in the adsorption of methylene blue and bromophenol blue dye in binary aqueous solution: using ultrasound power and optimization by central composite design. *J Mol Liq* 219:667–676. <https://doi.org/10.1016/j.moliq.2016.03.050>
61. Arfi RB, Karoui S, Mougin K, Ghorbal A (2017) Adsorptive removal of cationic and anionic dyes from aqueous solution by utilizing almond shell as bioadsorbent. *Euro-Mediterr J Environ Integr* 2:20. <https://doi.org/10.1007/s41207-017-0032-y>
62. Ahmad R, Mondal PK (2009) Application of acid treated almond peel for removal and recovery of brilliant green from industrial wastewater by column operation. *Sep Sci Technol* 44(7):1638–1655. <https://doi.org/10.1080/01496390902775836>

Publisher's Note Springer Nature remains neutral with regard to jurisdictional claims in published maps and institutional affiliations.